10-1-2004

Failure Analysis of the US 422 Girder Fracture

Eric J. Kaufmann

Robert J. Connor

John W. Fisher

Failure Analysis of the US 422 Girder Fracture

Final Report

By

Eric J. Kaufmann

Robert J. Connor

John W. Fisher

ATLSS Report No. 04-21

October 2004

ATLSS is a National Center for Engineering Research
on Advanced Technology for Large Structural Systems

117 ATLSS Drive
Bethlehem, PA 18015-4728

Phone: (610)758-3525
Fax: (610)758-5902

www.atlss.lehigh.edu
Email: inatl@lehigh.edu

Failure Analysis of the US 422 Girder Fracture

Final Report

By

Erik J. Kaufmann
Senior Research Engineer
ATLSS Engineering Research Center

Robert J. Connor
Research Engineer
ATLSS Engineering Research Center

John W. Fisher
Professor Emeritus of Civil Engineering
Lehigh University

ATLSS Report No. 04-21

October 2004

ATLSS is a National Center for Engineering Research
on Advanced Technology for Large Structural Systems

117 ATLSS Drive
Bethlehem, PA 18015-4728

Phone: (610)758-3525
Fax: (610)758-5902

www.atlss.lehigh.edu
Email: inatl@lehigh.edu

Table of Contents

1.0 Introduction

In 2003 a fracture was detected in a steel plate girder in a span of the bridge carrying US 422 over the Schuylkill River in Pottstown, PA. The fracture was found while retrofits to lateral gusset connections were being performed, similar to those that developed fractures in the Hoan Bridge, Milwaukee, Wisconsin in December 2000 [1]. The fracture occurred at one of these lateral gusset plate connections and resulted in a fracture of the girder web that propagated through the entire bottom flange and extended about nine inches into the web before arresting. Views of the fractured girder and lateral gusset plate connection are shown in Figures 1 and 2. The fracture was located at the intersection of the welds joining the lateral gusset plate and vertical stiffener to the web as was also observed in the Hoan Bridge. The lateral gusset plate also developed a fracture along the fillet weld joining the gusset plate to the vertical stiffener that propagated in the gusset plate for another six inches before arresting.

The fracture region of the girder was removed and delivered to the ATLSS Laboratories for evaluation of the fracture. The compositional, tensile, and fracture properties of the girder elements were determined and a fractographic examination of the fracture was performed to identify the fracture origin and initiation and propagation mechanism(s) in order to assess the possible causes of the fracture.

2.0 Fracture Examination

2.1 Visual Examination

The fracture region removed from the plate girder is shown in Figure 3 and consisted of the entire web and flange fracture including the lateral gusset fracture. Prior to removal from the structure a core was drilled at the arrested web crack tip to prevent possible re-initiation of the crack. The core was also included for examination (see Sec.II.3). Figure 4 shows the general appearance of the crack surface. A light corrosion layer was evident over most of the surface from exposure to the weather prior to removal. No evidence of heavy corrosion resulting from long-term exposure was seen anywhere on the crack surface which precluded the existence of an earlier crack in the gusset-vertical stiffener weld (see Figure 5) or girder web. Chevron marks on the web fracture surface clearly pointed to the weld intersection of the lateral gusset plate and the vertical stiffener as the origin of the girder fracture (see Figure 4). The brittle fracture propagated into the bottom flange via the girder longitudinal fillet welds (see Figure 6) and also propagated upward in the web until it arrested about 9 inches from the bottom flange.

The origin of the brittle fracture in the gusset-vertical stiffener fillet weld appeared to be in the vicinity of the weld intersection (within 1in.), however, its point of origin was less clear since the weld quality was poor and multiple initiations occurred along the weld before arresting in the gusset plate beyond the vertical stiffener. The cause of the poor weld quality appeared to be due to excessive root opening between the gusset and the vertical stiffener from poor fit-up. It is apparent in the detailed view of the web fracture origin shown in Figure 4 that the gusset-vertical stiffener weld crack and web crack were offset about ¼ in. and not continuous and hence required a separate but near simultaneous brittle fracture initiation in each element.

Figure 7 shows a detailed view of the crack surface at the lateral gusset-vertical stiffener weld intersection after cleaning corrosion and debris from the surface. A shear lip at the termination of the gusset-vertical stiffener weld crack is also apparent consistent with two

separate fractures noted above. It is also clear from convergence of chevron marks that the origin of the web fracture was located in the weld metal at the corner intersection of the gusset-web weld and the gusset-vertical stiffener weld. Incomplete fusion and entrapped slag are also evident at the weld root and toe that is not uncommon at welds intersecting at corners. A cross-section of the weld joining the gusset plate to the web near the corner weld intersection is shown in Figure 8 and indicates the weld root condition in this region.

2.2 SEM Examination of Fracture Origin

The web fracture origin region was examined microscopically with a scanning electron microscope (SEM) to identify the presence and source of an initiating defect at the onset of crack instability. Figure 9 shows a low magnification SEM image of the origin region (also see Figure 7). Other than several sub-millimeter sized weld porosity defects no evidence of an initial fabrication defect was observed in this region. There was also no evidence of fatigue crack development in this region from surface or internal discontinuities present. The only fracture mechanism observed in this area was cleavage fracture as shown in the higher magnification image in Figure 9.

The absence of evidence of stable crack growth at the fracture origin is similar to the Hoan Bridge girder fractures at similar details [1]. In this case fracture was attributed to constraint induced fracture from high levels of tri-axial constraint at the crack-like geometrical condition at the weld intersection of the gusset plate and vertical stiffener elevating stresses well beyond the yield point in this region and stress intensities exceeding the fracture toughness of the web material. Although direct evidence of defect sharpening by cyclic stresses was also not observed in this case it was concluded that this had likely occurred at the microscopic level prior to the fracture. The similarity of the detail and absence of stable crack extension in the current fracture is suggestive of a similar fracture mechanism.

2.3 Web Crack Arrest

The core drilled at the web crack tip was examined fractographically to characterize the conditions that caused the fracture to arrest. Views of the core containing the crack tip and the exposed crack surfaces after saw-cutting and fracturing the remaining ligament at low temperatures is shown in Figure 10. It is clear that the cleavage fracture arrested due to the presence of two plate de-laminations that relieved the thickness constraint needed for continued propagation of the cleavage fracture. The SEM images seen in Figure 11 show that the cleavage fracture mechanism momentarily reverted to a ductile tearing mechanism just prior to arrest. It is also significant that prior to drilling the core the arrested crack re-initiated by fatigue and propagated about ¼ in. in the short time before the crack tip was removed from the structure. Figures 10 and 11 show the fatigue extension and typical fatigue striations observed in this region. At the observed growth rate a second fracture of the girder was highly probable in a short time interval.

2.4 Lateral Gusset Plate Crack Arrest

An enlarged view of the crack arrest region of the lateral gusset plate fracture is shown in Figure 12. A low magnification SEM image of the region is shown in Figure 13. As also observed at the web fracture crack tip the fracture mechanism also changed from cleavage to ductile tearing prior to arrest. Since no material discontinuities were observed at the crack tip to

alter the stress field in this region crack arrest occurred because of loss of crack driving force due to reduced stresses in the plate and arrest of the crack in the web.

3.0 Material Properties

3.1 Chemical Composition

A chemical analysis of the flange, web, and lateral gusset plate was performed to verify the steel grade of each plate material. The results of the analyses are provided in a lab test report included in Appendix A. All three plate materials conformed to the chemical requirements of ASTM A36 steel. The carbon, manganese, and residual element (P, S) content were typical of this grade of steel.

3.2 Mechanical Properties

The tensile and Charpy-v-notch (CVN) properties of the plate materials were measured to determine their strength and fracture toughness properties. Standard longitudinal tensile specimens were fabricated from the web and flange plate material in accordance with ASTM A370. Standard longitudinal full-size CVN specimens were fabricated from the 7/16" web and 1-1/4"flange in accordance with ASTM E-23. Three-fourths (7.5 mm) full-size specimens were fabricated fro the 3/8" gusset plate due to the limited plate thickness. The CVN specimens were tested over a range of temperatures to define the transition behavior of the steels.

Table 1 gives a summary of the tensile and CVN test results. The web and flange plate conformed to the strength requirements of ASTM A36 providing average yield points of 38 ksi and 35 ksi, and average tensile strengths of 62 ksi and 76 ksi, respectively. Although specimens were not tested from the gusset plate the composition indicated it was grade 36 steel and was assumed to possess strength consistent with this grade. Although only the flange satisfied the current AASHTO Zone 2 fracture critical toughness requirement for Grade 36 steel of 25 ft-lbs @ 40 F, the web and gusset plate were marginal. It is important to note that these requirements were not in place when the bridge was fabricated.

	Yld. Strength (ksi)	**Tensile Strength (ksi)**	**Elong. (2") (%)**	**CVN Energy** (ft-lbs)						
				0 F	**40 F**	**73 F**	**90 F**	**110 F**	**120 F**	**150 F**
Flange	34.5 36.0	74.0 77.5	34.6 32.7	4.0 6.0 14.5	27.0 26.0 25.0	31.0 45.5 42.0	46.5 38.0 40.5		54.5 61.5 57.0	
Web	38.3 38.3	61.5 62.0	37.9* 39.0*	8.5 5.5 6.5	18.0 29.0 15.0	45.0 59.0 51.0	74.5 69.5 65.5		76.0 74.5 72.0	
Gusset**	N/A	N/A	N/A	6.7 6.7 4.0	14.7 14.7 13.3	25.3 22.7 20.0		33.3 34.0 33.3		34.7 37.3 34.7

* 1 in. G.L.

** ¾ Size CVN, Equivalent Full-Size Energy Shown

Table 1 - Girder Tensile and CVN Test Results

A plot of the CVN test results obtained over a range of temperatures is shown in Figure 14. For all three plates the notch toughness was at or approaching upper shelf at room temperature and hence the static fracture toughness of the steels would be expected to remain high at temperatures as low as the minimum service temperature (0 to-30 F). An estimate of the fracture toughness, K_{IC} (1 sec), corresponding to bridge loading rates can be obtained by applying a K_{Id} –CVN correlation and temperature shift to the CVN test data. For the measured yield strength of about 38 ksi results in a full static temperature shift

$$T_{shift} = 215 - 1.5\sigma_y$$
$$T_{shift} = 158 \text{ F}$$

Using a ¾ shift for intermediate loading rates applicable to bridges, results in a reduced temperature shift of 119 F. Therefore, at the minimum service temperature range of 0 F the fracture toughness, K_{IC} (1 sec), can be estimated from the CVN test data obtained at 120 F. Applying the K_{Id} –CVN correlation

$$K_{Id} = [5E\ (CVN)]^{1/2} \qquad (1)$$

to the web CVN data at 120 F (i.e. 72 ft-lbs) results in a fracture toughness at intermediate loading rates, K_{IC} (1 sec) = 104 ksi$(in)^{1/2}$ at a service temperature of 0 F. A similar analysis for the flange and gusset plate material results in a fracture toughness at intermediate loading rates, K_{IC} (1 sec) = 90 ksi$(in)^{1/2}$ and 70 ksi$(in)^{1/2}$ respectively at a service temperature of 0 F.

4.0 Fracture Analysis

Since it appeared that the crack may have initially became unstable at the lack of fusion defect in the low quality gusset plate-vertical stiffener weld joint where an edge crack condition existed with a depth of about 0.25 in., the resulting stress intensity would be expressed as:

$$K = (1.12)\ \sigma\ (\pi a)^{1/2}\ F_w \qquad (2)$$

where $F_w = [\sec\ (\pi a_r/2t)]^{1/2}$ is a finite width correction factor, t is the thickness of the gusset plate (i.e. 3/8 in.) , σ is the yield point of the weld metal (about 55 ksi), and a =0.25 in. This yields a stress intensity, K, of about 77 ksi$(in)^{1/2}$ which likely exceeded the weld metal toughness at temperatures near the minimum service temperature. This resulted in a through-thickness crack analogous to the condition that existed at the Hoan Bridge and also to the Lafayette Street Bridge [2] after fracturing by fatigue.

In the Hoan Bridge analysis [1] the extension of the crack-like geometrical condition introduced by the slotted gusset plate at the weld intersection of the gusset and vertical stiffener into the web was modeled as a penny shaped crack with an effective crack width of 3 in. (see Figure 15). The stress intensity factor is defined as

$$K = (2/\pi)\ \sigma\ (\pi a_r)^{1/2}\ F_w \qquad (3)$$

where $F_w = [\sec (\pi a_r/2t)]^{1/2}$ is a finite width correction factor , a_r is the radius of the circular shaped crack, and $2t = 2a_r + 2t_w$. Substituting the web thickness, $t_w = 7/16$" and $2a_r = 3$ in. into Eq. 3 results in a stress intensity factor at the web plate surface

$K = (2/\pi)\ \sigma\ (\pi(1.5))^{1/2}\ [\sec (\pi(1.5)/3.875)]^{1/2}$
$K = \sigma\ (2.33)$
Using the yield point of the web $\sigma_y = 38$ ksi results in a maximum stress intensity, $K_{max} = 89$ ksi$(in)^{1/2}$.

The brittle fracture of the gusset-vertical stiffener weld would have imparted a dynamic load to the crack-like condition at the intersection of the gusset plate and vertical stiffener. For this case the dynamic fracture resistance of the web at the minimum service temperature of 0 F can be estimated from the CVN test data (i.e. 6 ft-lbs). Substituting into Eq. 1 results in a dynamic fracture toughness $K_{Id} = 30$ ksi$(in)^{1/2}$. Hence, the maximum stress intensity at the crack-like geometrical condition far exceeded the dynamic fracture resistance of the web and therefore a crack instability developed in the web nearly simultaneously after the gusset plate fillet weld fractured. A single dynamic event is also consistent with fracture of the web in the absence of fatigue crack sharpening at the crack origin.

5.0 Summary

1. The material properties of the web, flange, and gusset plates were found to conform to ASTM A36 steel. The fracture toughness of the plate elements satisfied or exceeded the current AASHTO Zone 2 toughness requirements for this grade of steel.

2. Fractographic examination of the girder fracture indicated that brittle fracture developed at two separate locations at the lateral gusset connection detail nearly simultaneously. A brittle fracture of the gusset plate vertical stiffener fillet weld and a brittle fracture of the web developed at the intersection of the gusset plate and vertical stiffener weld.

3. The web fracture propagated into the bottom flange via the girder longitudinal fillet welds and completely severed the bottom flange. The web fracture also propagated upward in to the web for a distance of about 9 in. before arresting at discontinuities in the web plate.

4. A fracture mechanics analysis of the crack-like conditions existing at both fracture origins indicated that the gusset plate fillet weld likely fractured under an unusual loading at low ambient temperatures and imparted a dynamic load to the crack-like condition at the intersection of the gusset plate and vertical stiffener which exceeded the dynamic fracture resistance of the web plate material at that temperature.

6.0 References

1. Wright, W.J., Fisher, J.W., Kaufmann, E.J., "Failure Analysis of the Hoan Bridge Fractures", Recent Developments in Bridge Engineering, Mahmoud (ed.), Swets & Zeitlinger, Lisse, 2003.

2. Fisher, J.W. Fatigue and Fracture in Steel Bridges: Case Studies, John Wiley & Sons, 1984.

Figure 1 - Fractured Bottom Flange of Girder and Arrested Web Fracture.
(Photo Courtesy of Gannett Fleming)

Figure 2 - View of Lateral Gusset Plate Connection and Fracture at the Weld Intersection of the Gusset and Vertical Stiffener Plates to the Web.
(Photos courtesy of Gannett Fleming)

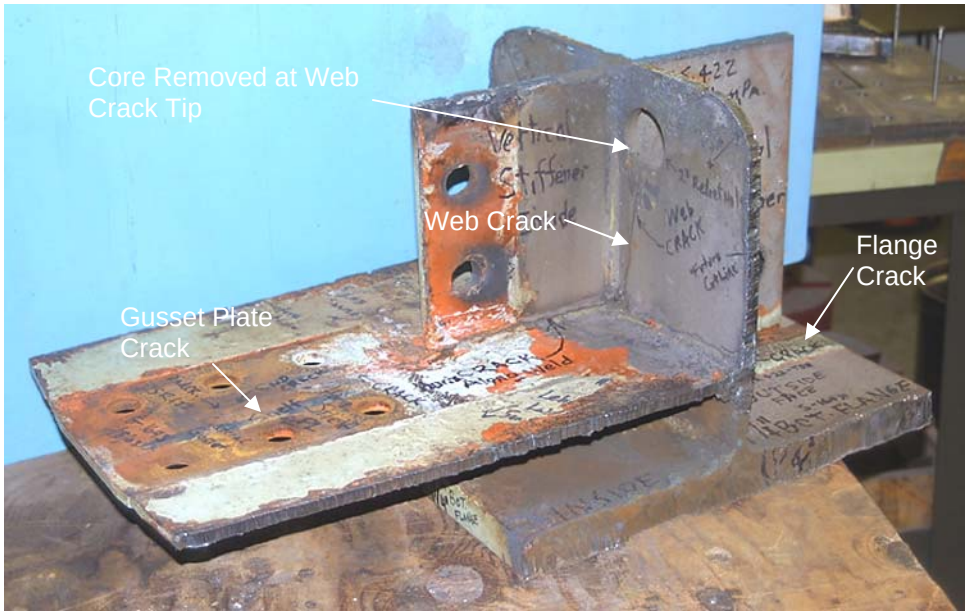

Figure 3 - Fracture Region Removed From the Girder.

Figure 4 - Brittle Fracture Appearance of Crack Surfaces With Chevrons Pointing Back to Fracture Origin at the Weld Intersection of the Lateral Gusset and Vertical Stiffener.

Figure 5 - Brittle Fracture Appearance of Gusset Plate-Vertical Stiffener Fillet Weld.

Figure 6 - Propagation of the Brittle Fracture From the Web Into the Bottom Flange Plate Via the Girder Longitudinal Fillet Welds.

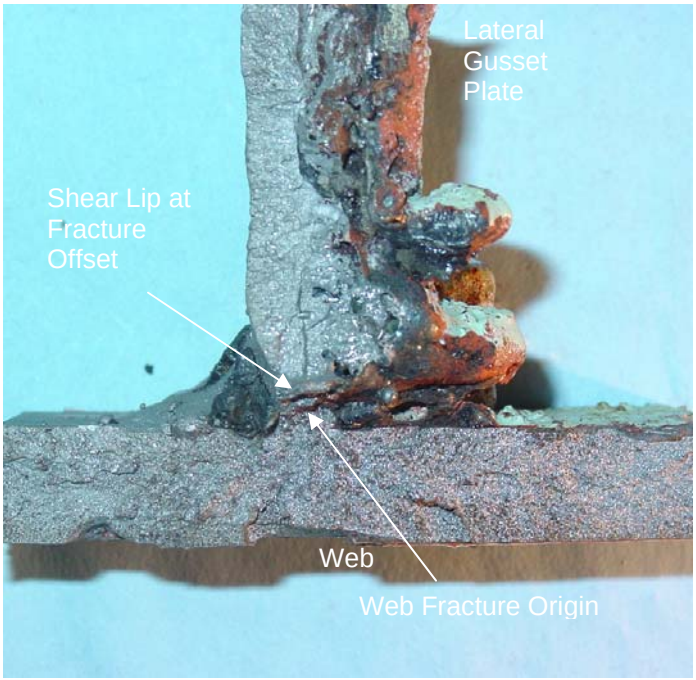

Figure 7 - Fracture Origin of Girder Fracture at the Intersection of the Lateral Gusset and Vertical Stiffener Welds.

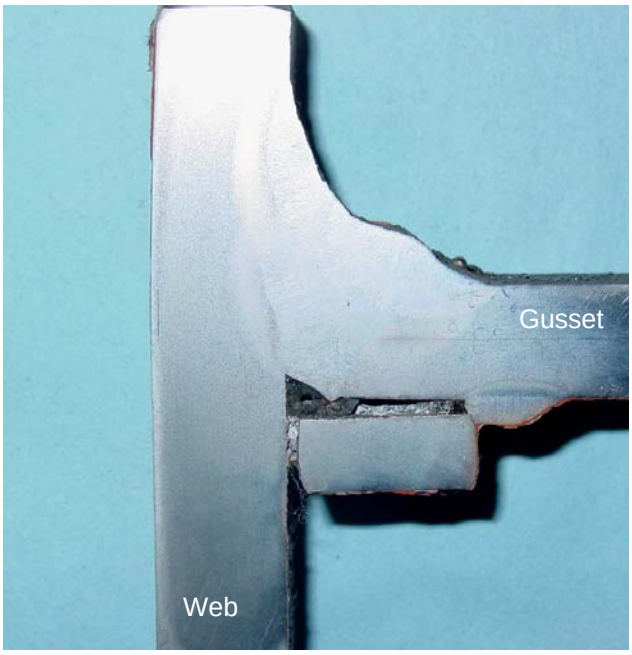

Figure 8 - Cross-section of Weld Joining the Gusset Plate to the Girder Web Showing Incomplete Root Fusion and Attendant Root Discontinuities.

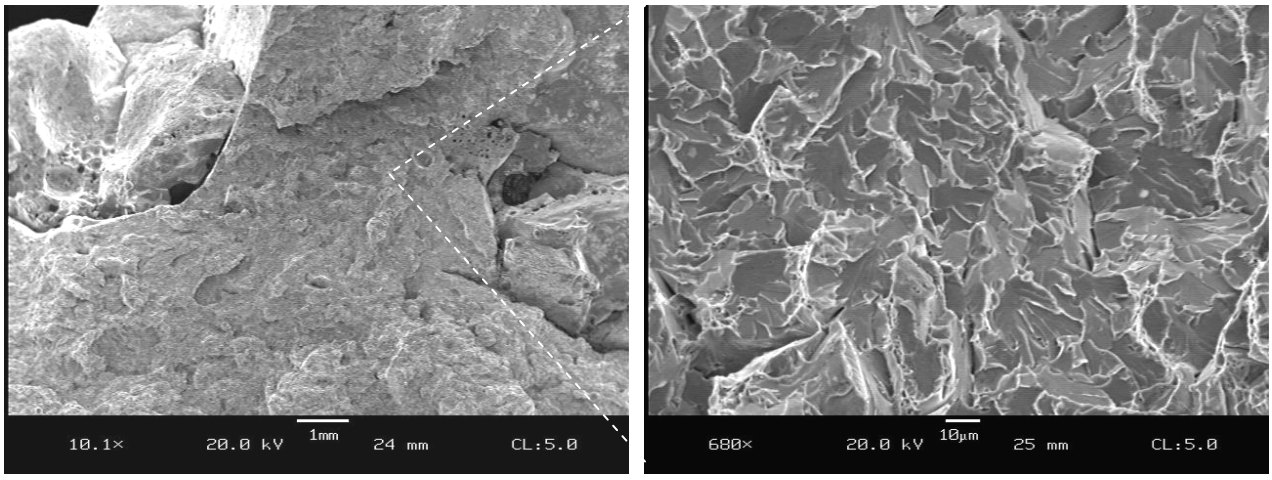

Figure 9 - SEM Images of the Fracture Origin Region and Cleavage Fracture. [Mag. 10.1x & 600x]

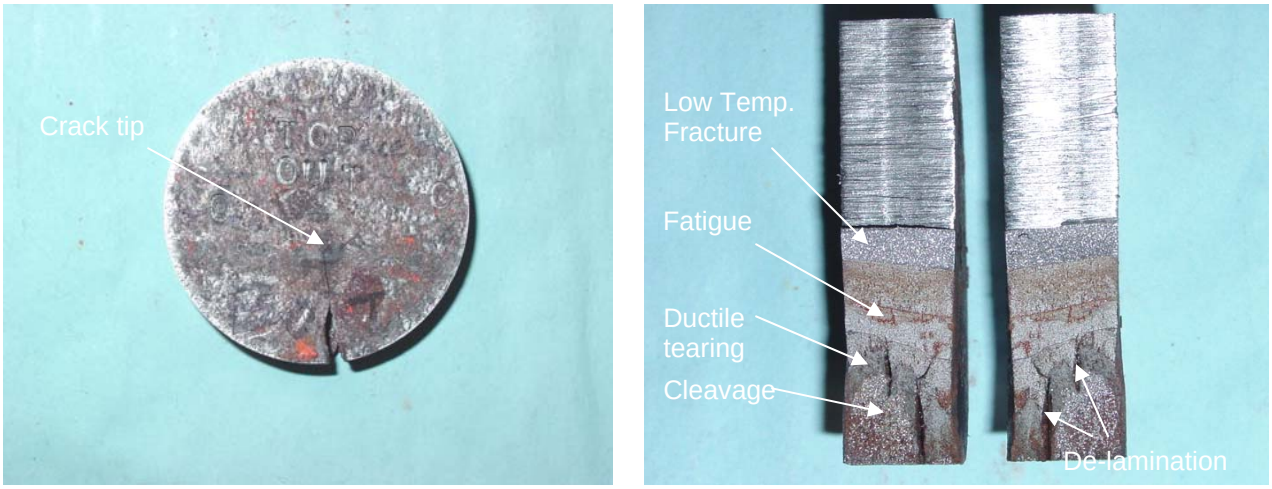

Figure 10 - Crack Tip of Web Fracture Arrested By Plate De-laminations. Note Fatigue Crack Extension Prior To Drilling Core.

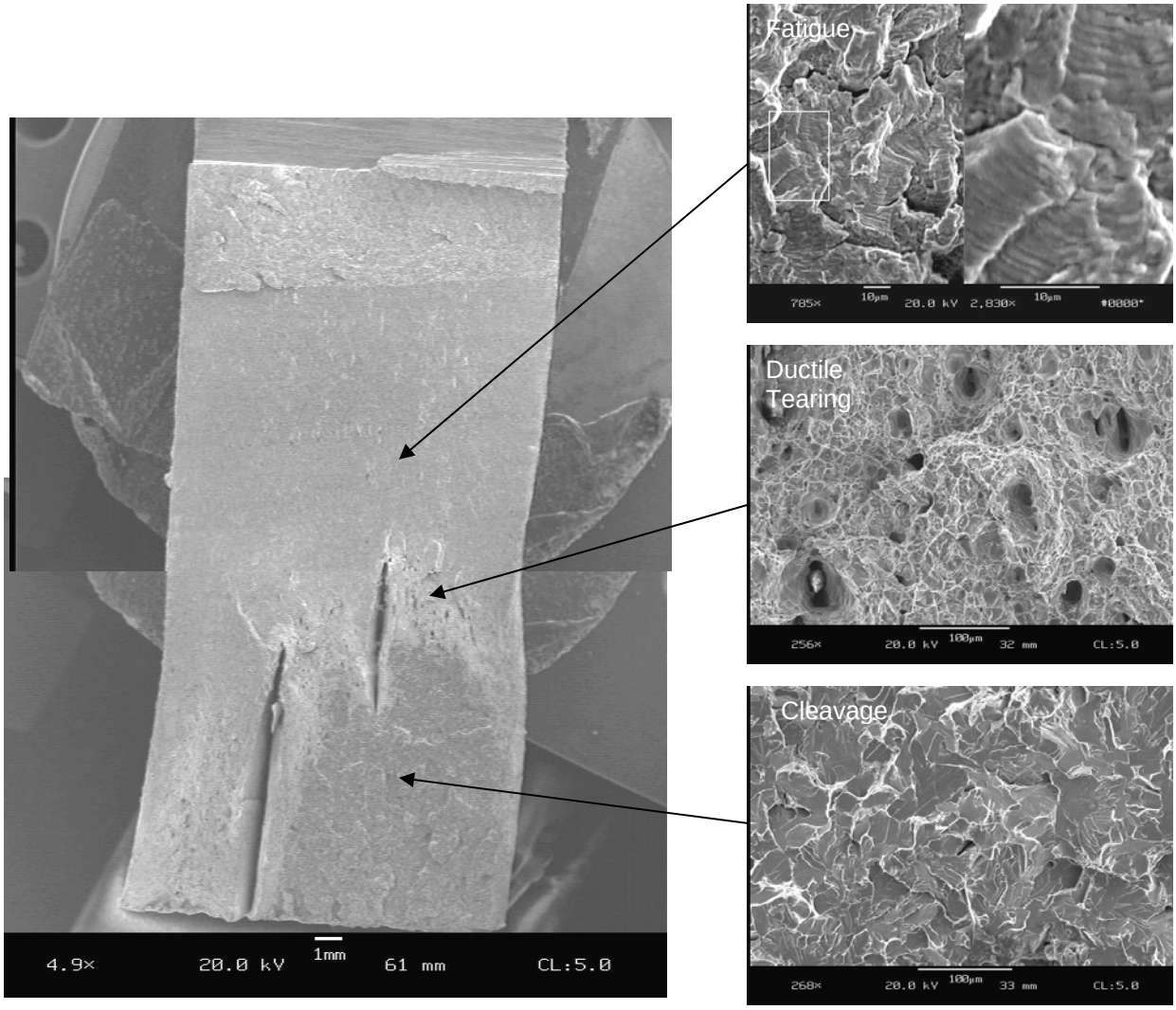

Figure 11 - SEM Images of Web Crack Tip Showing the Arresting De-laminations and Fracture Mechanism Details.

Figure 12 - Crack Arrest Region in the Lateral Gusset Plate.

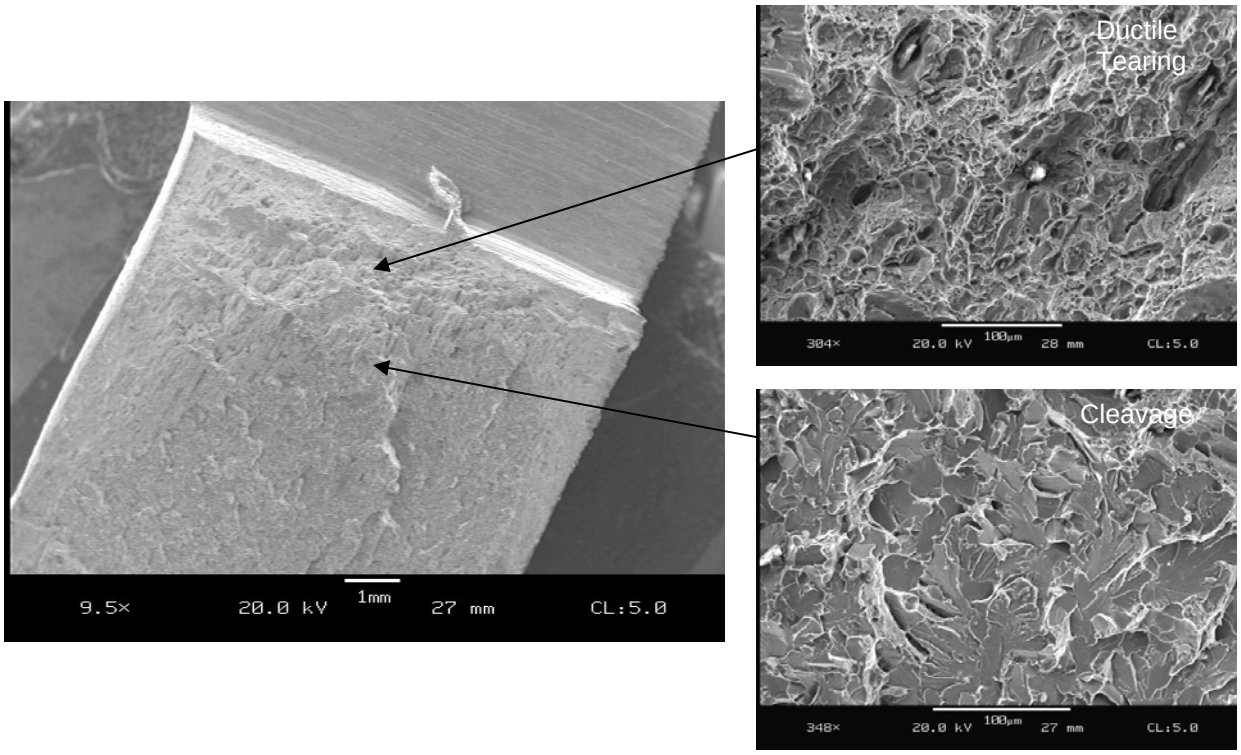

Figure 13 - SEM Images of the Gusset Plate Crack Tip Arrest Region.

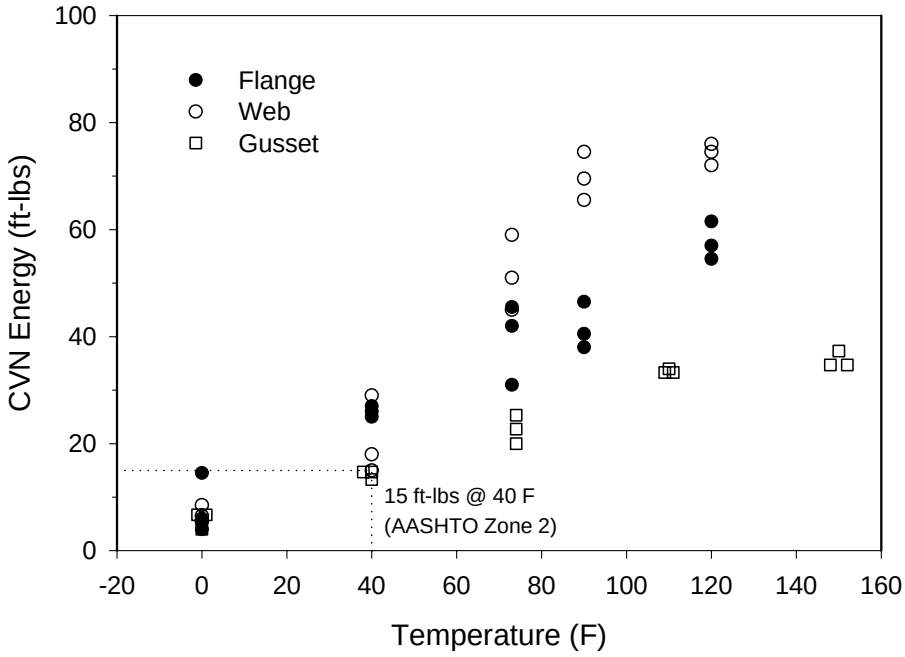

Figure 14 - CVN Test Results for the Girder Plate Elements.

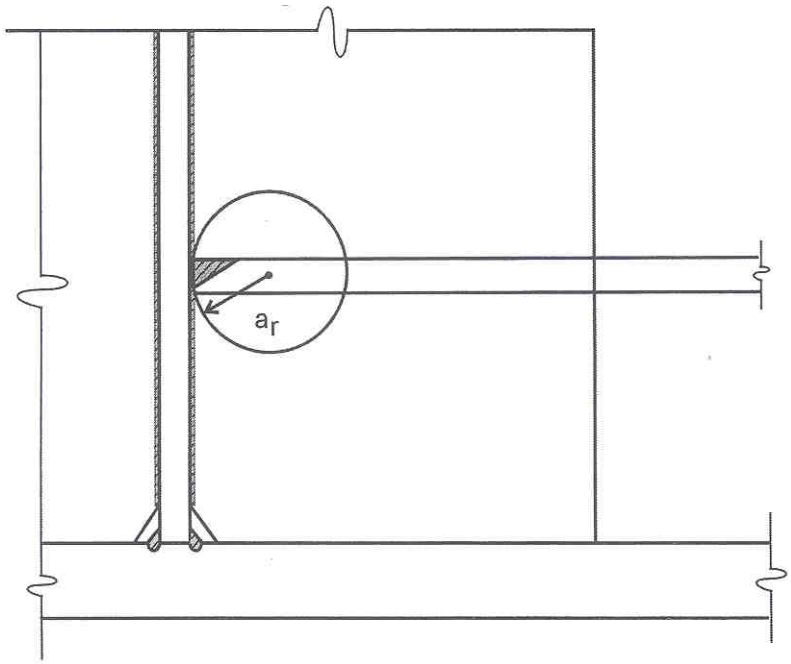

Figure 15 - Idealized Circular 3D Crack Model at Lateral Gusset Plate-Vertical Stiffener Intersection. [1].

Appendix A

Certified Test Report

LABORATORY TESTING INC.
2331 Topaz Drive, Hatfield, PA 19440
TEL: 800-219-9095 • FAX: 800-219-9096

LHU001-03-10-24689-1

A2LA ACCREDITED Cert. # 0117-01. 02. 03. 04

NADCAP Accredited Materials Testing Laboratory NDT (PT, MT, RT, UT)

SOLD TO
Lehigh University
520 Brodhead Avenue
Bethlehem, PA 18015-3008

SHIP TO
Lehigh University
ATLSS Engr. Research Center
117 ATLSS Dr., lmbt Lab.
Bethlehem, PA 18015
ATTN: Eric J. Kaufmann

CUSTOMER P.O.	CERTIFICATION DATE	SHIP VIA
43782	10/17/2003	EMAIL AND MAIL

DESCRIPTION

3 Test Samples, Steel, Sample ID Flange; Web and Gusset

Reference: Accnt. No. 526199 AT131.1, Accnt. Code 74060

Three samples were analyzed in accordance with Customer's Instructions with the following results:

ELEMENT	FLANGE	WEB	GUSSET
Al	0.003%	0.002%	0.006%
C	0.26%	0.13%	0.17%
Cr	0.052%	0.023%	0.027%
Cu	0.061%	0.026%	0.035%
Mn	0.80%	0.56%	0.47%
Mo	0.038%	0.025%	0.022%
Nb	< 0.001%	< 0.001%	< 0.001%
Ni	0.014%	0.010%	0.013%
P	0.013%	0.005%	0.005%
S	0.019%	0.012%	0.013%
Si	0.12%	0.003%	0.061%
V	0.003%	0.002%	0.002%

MERCURY CONTAMINATION: During the testing and inspection, the product did not come in direct contact with mercury or any of its compounds nor with any mercury containing devices employing a single boundary of containment.

NOTE: The recording of false, fictitious or fraudulent statements or entries on this document may be punished as a felony under Federal Statutes including Federal Law, Title 18, Chapter 47.

Sherri L. Scheifele
QA Coordinator
By: Sherri L. Scheifele
Authorized Signature